AD-A153 445 LOCAL PROPELLER BLADE FLOWS IN UNIFORM AND SHEARED ONSET FLOWS USING LDV (.. (U) DAVID W AAYLOR NAVAL SHIP RESEARCH AND DEVELOPMENT CENTER BET..

1/1

UNCLASSIFIED S D JESSUP ET AL. FEB 85 DTNSRDC-85/007 F/G 14/2 NL

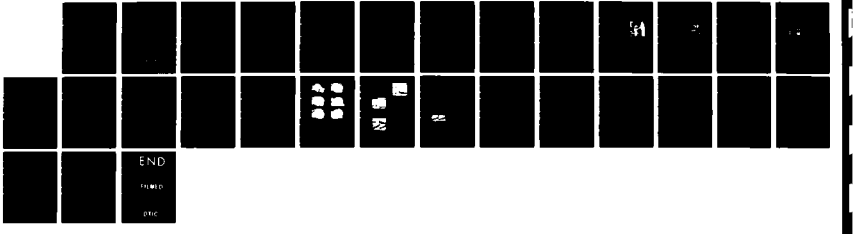

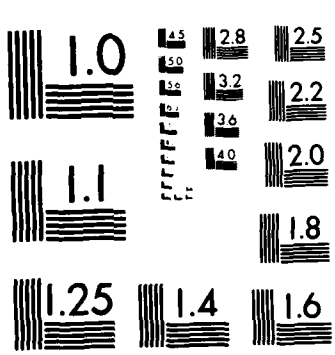

DTNSRDC-85/007

LOCAL PROPELLER BLADE FLOWS IN UNIFORM AND SHEARED ONSET FLOWS USING LDV TECHNIQUES

DAVID W. TAYLOR NAVAL SHIP RESEARCH AND DEVELOPMENT CENTER

Bethesda, Maryland 20084-5000

LOCAL PROPELLER BLADE FLOWS IN UNIFORM AND SHEARED ONSET FLOWS USING LDV TECHNIQUES

by

S.D. Jessup
C.G. Schott
M.F. Jeffers
S. Kobayashi

APPROVED FOR PUBLIC RELEASE: DISTRIBUTION UNLIMITED

Presented at the 15th ONR Symposium
Hamburg, Germany
September 1984

SHIP PERFORMANCE DEPARTMENT
RESEARCH AND DEVELOPMENT REPORT

February 1985

DTNSRDC-85/007

MAJOR DTNSRDC ORGANIZATIONAL COMPONENTS

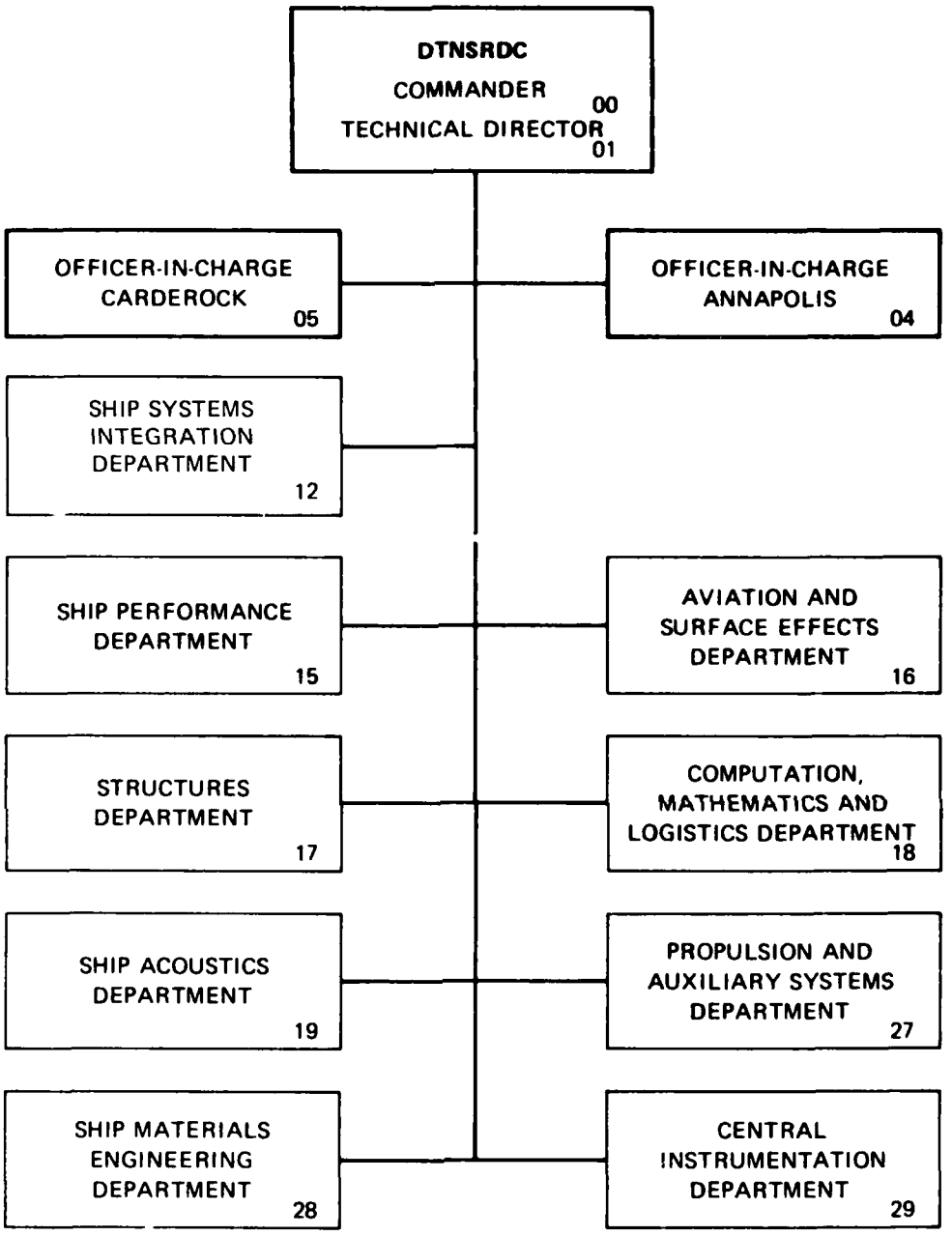

UNCLASSIFIED

SECURITY CLASSIFICATION OF THIS PAGE *(When Data Entered)*

REPORT DOCUMENTATION PAGE

READ INSTRUCTIONS BEFORE COMPLETING FORM

1. REPORT NUMBER: DTNSRDC-85/007	2. GOVT ACCESSION NO.
3. RECIPIENT'S CATALOG NUMBER	
4. TITLE *(and Subtitle)*: LOCAL PROPELLER BLADE FLOWS IN UNIFORM AND SHEARED ONSET FLOWS USING LDV TECHNIQUES	5. TYPE OF REPORT & PERIOD COVERED: Final
	6. PERFORMING ORG. REPORT NUMBER
7. AUTHOR(s): S.D. Jessup, M.F. Jeffers, C.G. Schott, S. Kobayashi	8. CONTRACT OR GRANT NUMBER(s)
9. PERFORMING ORGANIZATION NAME AND ADDRESS: David Taylor Naval Ship R&D Center, Ship Performance Department (Code 15), Bethesda, Maryland 20084-5000	10. PROGRAM ELEMENT, PROJECT, TASK AREA & WORK UNIT NUMBERS: (See reverse side)
11. CONTROLLING OFFICE NAME AND ADDRESS: David Taylor Naval Ship R&D Center, Technical Director (Code 01), Bethesda, Maryland 20084-5000	12. REPORT DATE: February 1985
	13. NUMBER OF PAGES: 25
14. MONITORING AGENCY NAME & ADDRESS *(if different from Controlling Office)*	15. SECURITY CLASS. *(of this report)*: UNCLASSIFIED
	15a. DECLASSIFICATION DOWNGRADING SCHEDULE

16. DISTRIBUTION STATEMENT *(of this Report)*

APPROVED FOR PUBLIC RELEASE: DISTRIBUTION UNLIMITED

17. DISTRIBUTION STATEMENT *(of the abstract entered in Block 20, if different from Report)*

18. SUPPLEMENTARY NOTES

Presented at the 15th ONR Symposium, Hamburg, Germany, September 1984

19. KEY WORDS *(Continue on reverse side if necessary and identify by block number)*

Blade	Flow Visualization	Sheared Onset Flow
Blade Surface Pressure	LDV	Turbulence Intensity
Boundary Layer	Local Blade Velocities	Uniform Flow
Field Point Velocity	Propeller	

20. ABSTRACT *(Continue on reverse side if necessary and identify by block number)*

Laser Doppler Velocimetry techniques were used to measure local propeller blade flows in the DTNSRDC 24-inch water tunnel. Velocity measurements were made upstream, downstream, and between blades. Measurements were made near the blade surface to identify potential flow surface pressure coefficients and streamwise boundary layer profiles. Blade surface flow

(Continued on reverse side)

DD FORM 1 JAN 73 1473 EDITION OF 1 NOV 65 IS OBSOLETE

S N 0102-LF-014-6601

UNCLASSIFIED

SECURITY CLASSIFICATION OF THIS PAGE *(When Data Entered)*

(Block 10)

Program Element 61152N
Project Number ZR00001
Task Area Number ZP0230101
Work Unit 1544-367

(Block 20 continued)

visualization was correlated with the measured boundary layer characteristics. Blade pressure distributions and streamwise boundary layer growth were compared with theory. Exploratory velocity measurements were made ahead of a propeller operating in an axisymmetric sheared inflow, and velocity and thrust correlations were made with theory. Measured velocities about the propeller showed good agreement with potential theory ahead of the propeller with discrepancies occurring downstream of the propeller due to viscous effects. Measured boundary layer growth at mid-span of the propeller blade was approximated well by two-dimensional boundary layer theory. Boundary layer profile measurements verified the location of transition determined from flow visualization techniques.

TABLE OF CONTENTS

LIST OF FIGURES

Page

LIST OF TABLES

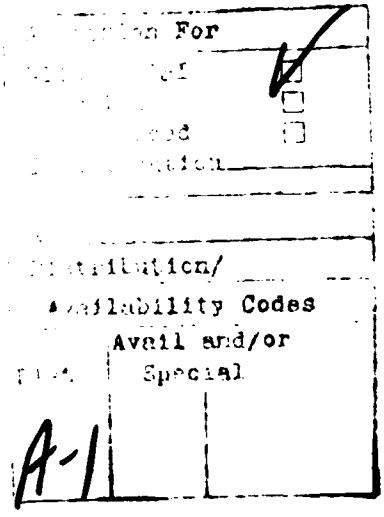

Local Propeller Blade Flows in Uniform and Sheared Onset Flows Using LDV Techniques

Stuart D. Jessup, Carl Schott,
Michael Jeffers and Sukeyuki Kobayashi

ABSTRACT

Laser Doppler Velocimetry techniques were used to measure local propeller blade flows in the DTNSRDC 24-inch water tunnel. Velocity measurements were made upstream, downstream, and between blades. Measurements were made near the blade surface to identify potential flow surface pressure coefficients and streamwise boundary layer profiles. Blade surface flow visualization was correlated with the measured boundary layer characteristics. Blade pressure distributions and streamwise boundary layer growth were compared with theory. Exploratory velocity measurements were made ahead of a propeller operating in an axisymmetric sheared inflow, and velocity and thrust correlations were made with theory. Measured velocities about the propeller showed good agreement with potential theory ahead of the propeller with discrepancies occuring downstream of the propeller due to viscous effects. Measured boundary layer growth at mid-span of the propeller blade was approximated well by two-dimensional boundary layer theory. Boundary layer profile measurements verified the location of transition determined from flow visualization techniques.

NOMENCLATURE

D = propeller diameter

c = chord length of propeller blade section

C_p = blade surface pressure coefficient, $(P-P_0)/1/2\ \rho V_r^2$, or $1-(\frac{V_b}{V_r})^2$

f = camber of propeller blade section

H = boundary layer shape factor, δ^*/θ

J = advance coefficient, V_A/nD

K_T = thrust coefficient, $T/\rho n^2 D^4$

K_Q = torque coefficient, $Q/\rho n^2 D^5$

n = propeller rotation speed, revolutions/second

p = propeller blade section pitch

P = pressure

P_0 = reference pressure

Q = torque

R = radius of propeller

r = radial distance from axis of propeller

T = thrust

V_A = speed of advance

V_b = velocity in the angle ϕ direction relative to the moving blade coordinate system, $V_\phi + 2\pi nr \cos\phi$

V_r = resultant inflow velocity to blade section $(V_A^2 + (2\pi nr)^2)^{1/2}$

V_s = representative ship speed in sheared wake DJ/n where J is determined from design K_T and open water performance data.

V_t = tangential velocity, positive in direction of rotation, average value at each blade angular position

V_ϕ = velocity in the direction of angle ϕ, average value at each angular position, $V_x \cos\phi + V_t \sin\phi$,

$$V_\phi = \frac{1}{n} \sum_{i=1}^{n} V_\phi(i)$$

$V_b(i)$,

$V_\phi(i)$ = velocity in the direction of angle ϕ, individual value at each angular position

x = axial position relative to propeller center plane, positive downstream

x_c = fraction of chord length

x_r = fraction of propeller radius

y = distance normal from surface

β = surface streamline angle with respect to potential flow streamline direction

δ^* = streamwise boundary layer displacement thickness

ρ = fluid density

ϕ = LDV velocity measurement direction, angle from vertical, positive upstream

ϕ_p = propeller blade section pitch angle

θ = streamwise boundary layer momentum thickness

ν = kinematic viscosity

$(\bar{-})$ = bar signifies mean value

1. INTRODUCTION

Recent advances in Laser Doppler Velocimetry have provided the ability to measure time-varying velocities near operating propellers. Pioneering work by Min (1978) established techniques and provided field point velocity measurements ahead of and behind operating propellers. Correlations made with Kerwin and Lee's (1978) numerical lifting surface theory, PUF-2, showed good predictions of field point velocity distributions ahead of the propeller and outside the slipstream. Inside the slipstream, downstream of the propeller, predictions showed significant discrepancies with measurements that were attributed to displacement effects due to the viscous wakes of the blades and inaccuracies in the numerical modeling of the downstream vortex system. Using the same LDV system, Kobayashi (1981) calculated the section drag of the blades from detailed measurements of the viscous wakes. Kerwin (1982) presented further correlations of field point velocities about operating propellers using a refined measuring technique resulting in improved spatial resolution. Comparisons were made with Greeley's (1982) improved lifting surface model, PSF-2, showing agreement similar to Min's results. Program FPV-10, reported by Kerwin (1979) was used to generate field point velocities from PSF-2.

All the LDV measurements described were conducted using a one component, dual beam, forward-scatter on-axis system. Transmitting and receiving optics were positioned on opposite sides of the water tunnel with a direct line of sight across the tunnel necessary to perform the measurements. This arrangement restricted the measurements to regions outside the swept area of the rotating propeller.

This paper describes measurements made about rotating propellers using a one component, dual beam, on-axis, backscatter LDV system. Measurements were made within the swept area of the propeller disk, in the potential flow regions between the blades, and within the blade boundary layer. High spatial resolution was obtained with small measuring volume optics in conjunction with precise angular positioning of the propeller. Flow visualization using oil dot techniques was conducted to correlate with measured blade boundary layer characteristics. Exploratory measurements were also made ahead of a propeller operating in an axisymmetric sheared wake to investigate effective wake and resulting propeller performance. The results of these experiments contribute to the understanding of the potential flow and boundary layer characteristics of typical propeller blade sections, and provide insight into the boundary layer displacement effects on the blade, and propeller operation in sheared wakes.

2. EXPERIMENTAL TECHNIQUES

2.1 Test Facility

Tests were conducted in the DTNSRDC 24-inch diameter (0.61m) water tunnel incorporating an open jet test section and a downstream drive system. A window insert was installed in the open test section as shown in Figure 1 to permit a close proximity of the LDV

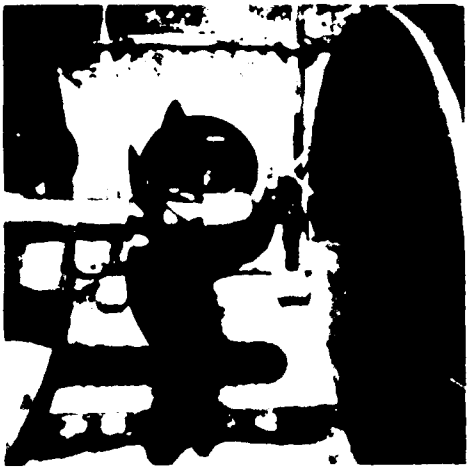

Figure 1 DTNSRDC 24 Inch Water Tunnel Open Jet Test Section With Tunnel Window Insert for LDV Measurements

optics to the blades of the propeller. This was necessary to minimize the focal length of the LDV optics system for maintaining a minimum measuring volume size. The extended window was positioned approximately 13 inches (33 cm) from the tunnel centerline and was estimated to induce an asymmetry to the uniform flow test section of less than 2%.

The primary propeller tested was DTNSRDC Model 4119. This is a 12 inch (30.5 cm) diameter three-bladed propeller described by Denny (1968), designed for uniform flow as a double thickness version of DTNSRDC propeller Model 4118. The propeller was tested at 7 and 14 rps at a nominal design J of 0.833 corresponding to a propeller Reynolds number of 0.7 and 1.4 million. Propeller geometry is shown in Table 1.

A relatively large, 150 Hp, dynomometer system was chosen for the tests to maximize shafting rigidity. This was necessary because of the large distance between the propeller and the location of the encoder measuring shaft angular position. It was thought that a rigid shaft arrangement would maximize the consistancy of the angular position measurement. Consequently, a compromise was made in the accuracy of thrust and torque measurements, since only 10 percent of the load capacity of the dynamometer was utilized.

TABLE 1 GEOMETRY OF DTNSRDC MODEL PROPELLER 4119

Diameter D 1.000 ft (0.305m)

Rotation Right Hand

Number of Blades 3

Hub Diameter Ratio D_h/D 0.20

Skew Rake None

Design Advance Coefficient J 0.833

Section thickness form NACA66 (DTNSRDC Modified)

Section Mean Line NACA a = 0.8

r/R	c/D	P/D	$\phi_{0.7R}$ (Degrees)	t/c	f/c
0.2	0.320	1.105	60.38	0.20550	0.01429
0.3	0.3625	1.102	49.47	0.15530	0.02318
0.4	0.4048	1.098	41.15	0.11800	0.02303
0.5	0.4392	1.093	34.84	0.09016	0.02182
0.6	0.4610	1.088	29.99	0.06960	0.02072
0.7	0.4622	1.084	26.24	0.05418	0.02003
0.8	0.4347	1.081	23.28	0.04206	0.01967
0.9	0.3613	1.079	20.88	0.03321	0.01817
0.95	0.2775	1.077	19.84	0.03228	0.01631
1.0	0.0	1.075	18.89	0.03160	0.01175

Propeller test conditions were set using thrust identity, where the propeller rpm was set and tunnel water speed was varied to produce measured open water thrust. Preliminary measurements of field point velocities ahead of Propeller 4119 showed a 3% difference in circumferential average axial velocity when compared with predicted values using PSF-2. This discrepancy was believed to be due to the combined effects of measured thrust error, a 1% difference in measured tunnel test section velocity compared to open water advance speed, and the approximate 2% reduction in tunnel test section velocity in the vicinity of the tunnel window insert. Therefore, all correlations were made assuming a 3% reduction in advance speed from the design condition, resulting in an assumed advance coefficient of 0.806. The comparison of the predicted and measured field point velocity distributions at the nominal and assumed advance coefficients are shown later in the paper.

2.2 Laser Doppler Velocimetry System

The LDV system used was a relatively conventional TSI, Inc. one component dual beam system operating in the on-axis back scatter mode. A Spectra-Physics 2 watt ion-argon laser was used, utilizing the green 514.5 nm wavelength line. The single beam was split into two coherent beams through a beam splitter. One beam was frequency shifted to distinguish velocity direction. A 2.27x beam expander was used with a 250 mm focal length lens with 50mm beam separation. This arrangement resulted in a measuring volume .0028 inches (.072mm) in diameter and .030 inches (.75mm) long with 28 fringes across the measuring volume. With the on axis arrangement, the received scattered light past back through the same optical system through a field stop for filtering extraneous scattered light, and then to a photomultiplier. The optical system was afixed to rotating mounts so the beam orientation and thus the direction of velocity measurement could be rotated about the beam axis. Figure 2 depicts the LDV system.

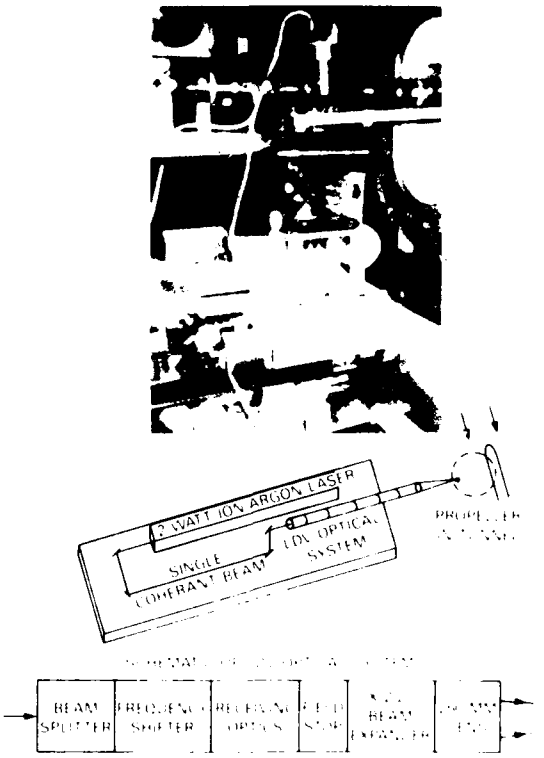

Figure 2 Laser Doppler Velocimetry System: Single Component, Dual Beam, On-Axis Back Scatter

The doppler signal from the photomultiplier output was processed with both a frequency tracker and a burst counter. Signals were initially band pass filtered to reduce noise. The tracker was used for alignment purposes, processing qualitative results, and identifying blade passage speed. The counter was used for quantitative data processing in conjunction with the computer.

For this test in the water tunnel the data processing rate of individual velocity measurements was relatively good, from 200 to 2000 processed measurements per second. The

data rate was dependent on optical alignment, velocity measurement direction, and tunnel seeding. Routinely, the tunnel water was filtered to 5 micron particle size and then seeded with 1.5 micron size silicon Carbide seeding material. The rate of the processed velocity measurements were considered random in nature so that data collection procedures responded to individual measurements and not to a prescribed time or blade angular position based on propeller rotation.

2.3 LDV System Positioning, Calibration and Accuracy

Positioning of the LDV system was performed with a manually controlled , three-directional traverse system as shown in Figure 2. Translations along the propeller shaft axis were performed by moving the entire LDV system, while vertical and horizontal translations from the propeller shaft axis were performed by moving the optical system relative to the single beam laser source. Vertical traverse was performed with an optical scissors jack. Position was measured manually with dial and vernier calipers to a resolution of 0.001 inches (.025mm).

The position of the LDV measuring volume was referenced to the geometry of the propeller inside the tunnel. The vertical position of the LDV measuring volume was referenced to the upper and lower edges of the propeller hub. The axial position was referenced to a mid-chord line drawn on a propeller blade while the propeller was stationary and was checked by positioning the measuring volume at the leading or trailing edges while the propeller was rotating. This was easily performed due to the large doppler signal produced when the measuring volume intersected the blade surface and provided a correction due to shaft system extension under load. The horizontal position from the propeller shaft centerline was referenced to lines of constant radius drawn on the propeller while stationary in the tunnel.

Calibrations were performed by measuring the surface speed of a disk rotating in place of the propeller in the water tunnel. Calculated and measured calibration factors differed by 3' with the difference thought to be due to deviations in the two beam separation distance at the lens.

Calibrations were checked through out the experiment by measuring the blade surface speed while rotating at test conditions. The magnitude of blade speed was most accurately determined using the tracker processor because of its narrow band width and the large offset between blade surface speed and the measured water velocity in the vacinity of the blades. On an average basis the check calibrations were within 1' of the original calibrations but varied up to 3.4' amongst all the measurements. This variation was due primarily to errors in the positioning horizontal to the propeller axis and the angle setting of the two laser beams from the vertical.

2.4 Procedure for Measuring Local Blade Velocities

A procedure was derived for measuring the streamwise velocity component near the blade surface using the one component LDV system. The streamwise direction is that tangent to a line of constant radius drawn on the blade. The dual beam LDV system measured the velocity in the plane of the two intersecting beams, perpendicular to the line bisecting the two beams. Figure 3 depicts the measurement of the blade streamwise velocity component.

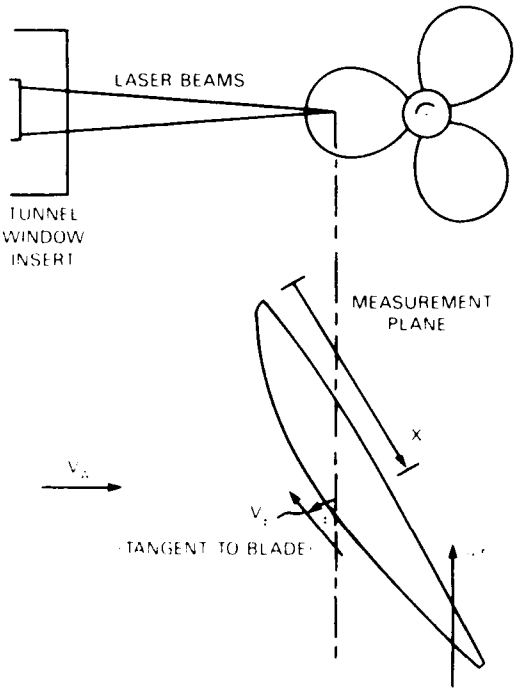

Figure 3 Measurement of Blade Streamwise Velocity

The measuring volume located at the intersection of the two beams was positioned at the horizontal centerline plane of the propeller. As the propeller rotated, the blade cut through the measuring volume at some point on the blade. The two beams were rotated about the optical center to orient the direction of velocity measurement to be tangent to one side of the blade as it passsed through the measuring volume. This arrangement resulted in a traverse diagonally through the blade surface boundary layer, measuring the velocity parallel to the blade surface at the point where the measuring volume intersected the blade. The mechanism for the boundary layer traverse was simply the rotation of the blade, since the LDV measuring volume remained stationary.

The angle that the two beams were rotated from the vertical, ϵ, was obtained analytically from the design propeller geometry. This angle was similar to the pitch angle of the blade section with a deviation with distance from the mid-chord line.

2.5 Measurement of Blade Angular Position

Each velocity measurement processed by the LDV system had to be associated with a given propeller blade angular position. When the tracker was used for qualitative measurements, the time sweep of a storage oscilloscope was used in conjunction with a single pulse per revolution from a magnetic pick-up to reference individual measurements to a known blade angular position. Figure 4 depicts a typical velocity distribution through the rotating propeller disk.

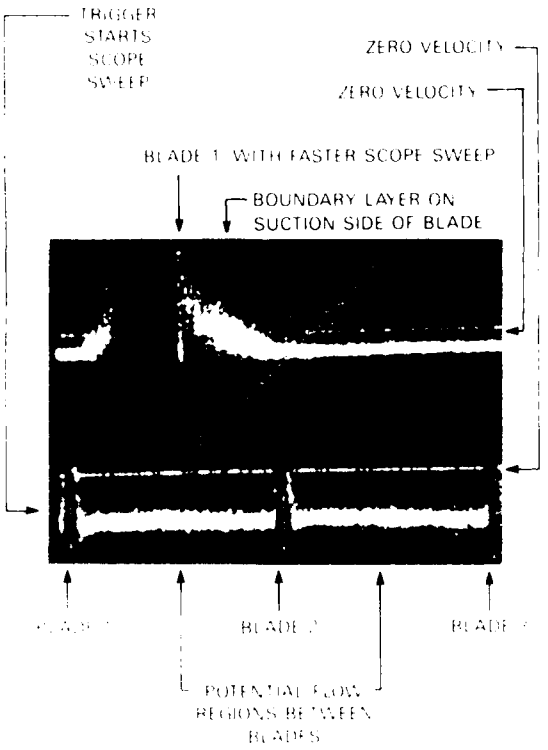

A digital output absolute positioning optical rotary encoder (BEI, #5V680HB) was used to measure blade angular position when quantitative data was collected by computer. A natural binary 12 bit resolution was output from the encoder corresponding to 4096 angular positions per revolution. An angular speed limit of 10 rps was prescribed with this resolution due to a 41 kHz frequency response of the optical components in the encoder, but a working limit of at least 15 rps was attained.

2.6 Computer Data Collection and Analysis

Processed LDV velocity measurement data from the burst counter were collected with a Perkin Elmer (Interdata) 7-16, 16 bit minicomputer. With each velocity measurement collected, an associated shaft angular position was read from the shaft encoder. Velocity and position data sets were transfered to 9 track-digital tape. A typical run, requiring ten minutes of test time consisted of 168,000 data sets with approximately 40 velocity measurements at each of 4096 angular positions.

Data on digital tape was transfered to a CDC 176 mainframe computer and stored on a cartridge type mass storage system. The velocity data were sorted by angular position and the mean velocity, standard deviation and number of data points at each angular position were retained for each analyzed run. A computer program was developed to analyze the velocity data in the regions close to the blade in a reference frame moving with the blades. The program calculated the blade pressure coefficient from the potential flow regions above the blade surface and calculated boundary layer characteristics of displacement thickness, shape factor, turbulence intensity and velocity profile.

When the measuring volume intersected the blade surface a relatively large signal was returned to the LDV processor. This resulted in a substantially larger number of data samples collected at the angular position corresponding to the blade surface. This phenomenon was used to locate the angular position of the blade surface to within one angular

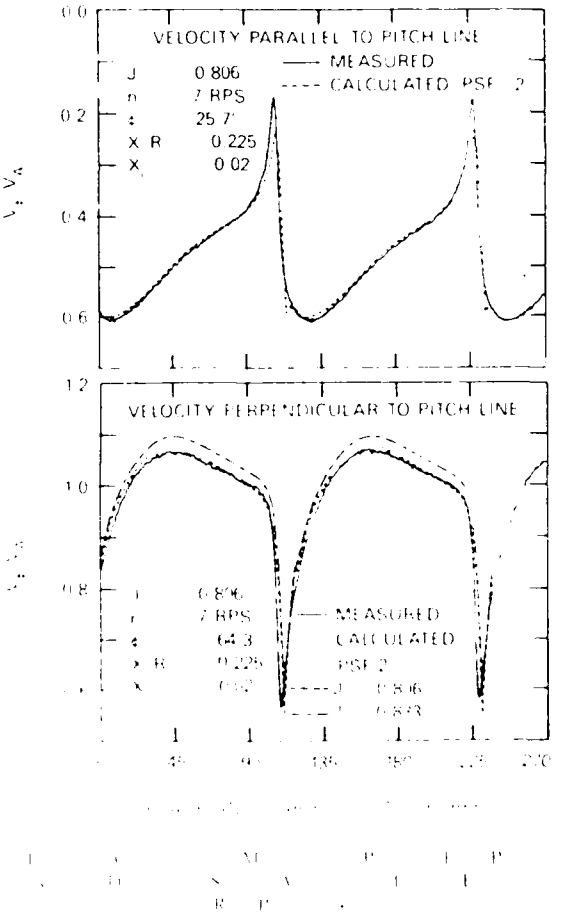

location.

The accuracy of the angular position corresponding to the blade surface had a significant effect on the accuracy of the measured boundary layer parameters. Near the leading edge, where only about six angular positions were contained within the boundary layer, a variation of one angular position produced a dramatic change in δ^* and H. To improve surface angle resolution, in cases where a large number of data samples were shared by two adjacent positions, boundary layer parameters were calculated for each of the adjacent surface angles and then averaged. From this procedure, surface angular resolution was improved to one half an angular location with a resulting estimated error in δ^* of $\pm 0.00021 Y/C$.

3. DISCUSSION OF EXPERIMENTAL RESULTS

3.1 Local Blade Flow Measurements About Propeller 4119

Initial measurements were made upstream of the propeller near the leading edge of the blades. As previously reported by Min (1978) and Kerwin (1982) LDV measurements of field point velocities in the potential flow regions ahead of the propeller correlated well with numerical predictions using lifting surface theory. Figure 5 shows the measured field point velocity distribution of propeller 4119 slightly ahead of the leading edge at the 0.7 radius. The measurements correspond to a vector decomposition of the traditionally measured axial and tangential velocity components into directions parallel and perpendicular to the blade section pitch line. Comparisons made with the propeller numerical lifting surface performance prediction program (PSF-2) showed good agreement with measurements. A reference phase for the field point velocity predictions was determined by shifting the phase of the predicted velocity distribution in Figure 5 to match the measured result. Figure 6 shows a composite of the blade to blade velocity distributions traversed axially through the propeller disk across the blade chord. The measurement direction is oriented parallel to the suction side blade surface at the intersection of the LDV measuring volume and the suction side surface. The velocity profiles shown are nondimensionized on V_r, the resultant inflow velocity at the given radial section. Velocity V_b represents the measured velocity V_ϕ transformed to the moving blade reference frame, where $v_b = V_\phi + 2\pi nr \cos\phi$.

The blanked-out regions in the plots correspond to the measuring point intersecting the interior of the blade. Measurements near the suction side of the blade are to the right of the blanked region and the pressure side is to the left. Over most of the chord length the velocity jump across the blade can be seen. Near the leading edge on the pressure side of the blade the flow is generally retarded near the stagnation point, but is accelerated near the blade surface downstream of the stagnation point. On the suction side near the trailing edge the surface velocity decelerates without any apparent flow separation.

The viscous boundary layers developed along each side of the blade are confined to the thin regions very close to the blade surfaces. Even near the trailing edge, the relatively thick boundary layers appear to have little effect on the overall potential flow velocity fields.

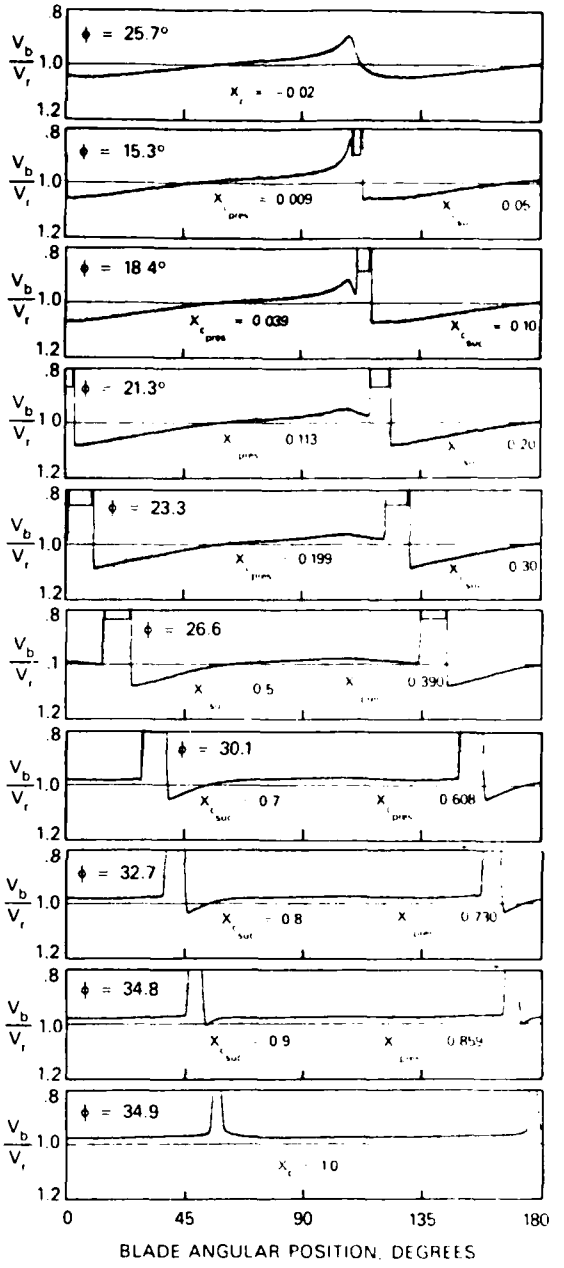

Figure 6 Measured Streamwise Potential Flow Velocity Profiles Through 0.7R of Propeller 4119

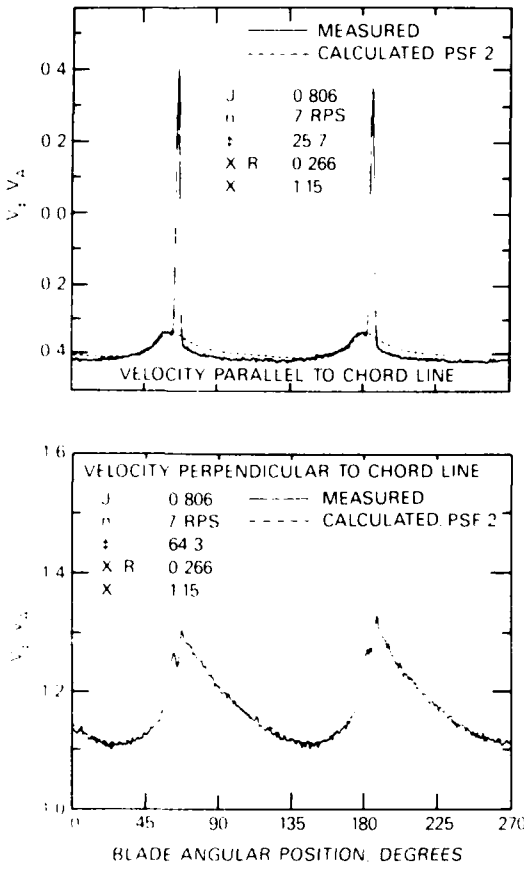

Figure 7 Comparison of Measured and Predicted Field Point Velocity Distribution Slightly Behind Trailing Edge at 0.7R of Propeller 4119

Figure 7 shows correlations of measurements with predictions downstream of the trailing edge. The influence of the viscous wake on the measured downstream field point velocity distribution can be seen. The viscous blade wake appears to increase the streamwise velocity parallel to the chordline, relative to the moving blade, while the velocity perpendicular to the chordline is reduced from the potential flow prediction. In the region between the blades, toward the pressure side of the blade, correlation with potential flow predictions is good.

3.2 Measured Blade Surface Pressure Distributions Derived from LDV Measurements

Blade surface pressure distributions were derived from the LDV measurements and compared to numerical lifting surface predictions. From the data shown in Figure 6, the potential flow velocity measured parallel to the blade surface, V_s, was extracted at the edge of the boundary layer, and referenced to the moving blade coordinate systems, (V_b). The pressure coefficient was then calculated using Bernoulli's equation for irrotational, uniform onset flow, nondimensionalized on the resultant inflow velocity, V_r.

$$C_p = 1 - (V_b/V_r)^2$$

Pressure distributions were derived from the measured results at the 0.7 radii of Propeller 4119. The streamwise blade surface angles, ϕ, were set to measure velocities tangent to the suction side of the blade. Pressure side pressure distributions were approximated from the suction side measurements. The technique has the capability to extract the potential flow surface velocities of each blade of the propeller. In this case, the measured pressure coefficients represent the average value for all blades.

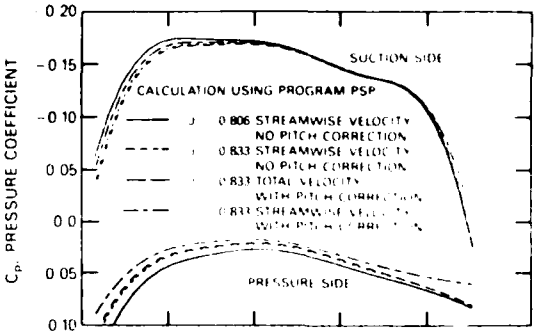

Figure 8a Calculation for Different Input Parameters

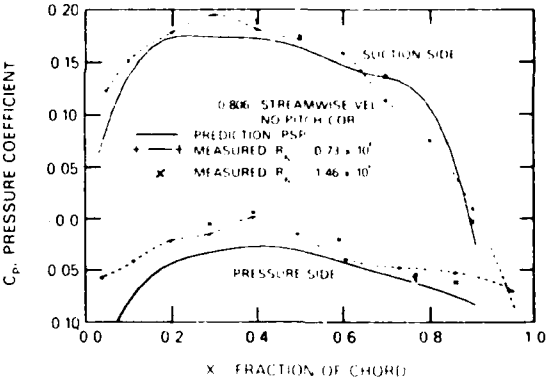

Figure 8b Comparison of Measured and Calculated Results

Figure 8 Pressure Distribution Derived From Measured Streamwise Potential Flow Velocity at 0.7R Propeller 4119 at 0 Deg With Correlation to PSP Predictions

Figure 8 shows the measured pressure coefficients at the 0.7 radius along with comparisons with numerical lifting surface theory (Kim and Kobayashi, 1984). Kim and Kobayashi's procedure signified by program PSP, uses the prediction procedure of Greely and Kerwin (1982) represented by program PSF-2 which also provided the field point velocity predictions. For these comparisons, PSP was modified to calculate pressure distributions based on the streamwise velocity components only, to be compatible with the LDV measurements. Figure 8a shows the variation in

pressure distribution predictions for variations in relevant PSP computer code input parameters. Little change resulted from computations based on the streamwise only and the total velocity along the blade surface at the 0.7 radius. The pitch correction adopted in PSF-2 is an empirical correction reducing pitch to account for viscous effects, and it was not considered in the correlation with measured results.

Figure 8b shows the experimental results compared to calculations. More extensive experimental results were recorded at the low Reynolds number of 7.3×10^5. Data show a reasonably faired distribution over the chord with some anomalies at midchord that could be due to experimental error or local unfaired geometry. The experimental distribution matches prediction reasonably well. The most obvious and accountable discrepancy occurs on the suction side of the blade over the latter part of the chord. There the calculated result underpredicts the measured value. This discrepancy is believed to be a boundary layer displacement thickness effect. The pressure distribution on the pressure side of the blade appears to be further from prediction than that on the suction side. This may be because the blade surface angle φ was set to measure velocities tangent to the suction surface. Hence, significant errors may have resulted near the leading and trailing edges where the suction and pressure side surface angles were different.

Measurements taken at the higher Reynolds number (1.46×10^6) show a closer agreement with the potential flow predictions as expected, due to the smaller influence of displacement thickness, especially in the region aft of midchord.

TABLE 2 PERFORMANCE PREDICTIONS FOR PROPELLER 4119

	J	K_T	$10\,K_Q$
Measured Open Water Test	0.833	0.150	0.285
	0.806	0.157	0.293
PSF 2 With Pitch Correction	0.833	0.151	0.282
	0.806	0.162	0.298
PSF 2 Without Pitch Correction	0.833	0.153	0.287
	0.806	0.164	0.303

3.3 Comparison of Measured and Predicted Thrust and Torque

Table 2 shows comparisons of measured and predicted thrust and torque for propeller 4119 at design J. Predictions using PSF-2 with a pitch correction for viscous effects were very close to measured open water test results, within 1% difference on thrust. The water tunnel test conditions were set by thrust identity based on the open water test results at a design J of 0.833. An effective J of 0.806 was established based on asymmetry in the inflow and possible errors in thrust measurement. Predictions at this advance coefficient showed a signficant discrepancy with the open water data. Further tests will include measurements of the inflow asymmetry and more careful load measurements to establish quantitative effects of viscosity on performance.

3.4 Boundary Layer Measurements

Boundary layer profiles were extracted from the streamwise velocity measurements at angular positions close to the blade surfaces. With the resolution of 4096 positions per revolution, data points through the boundary layer varied from four near the leading edge to sixty at the trailing edge. A diagonal traverse was obtained through the boundary layer at an angle of (90 - ϕ) degrees from the normal vector from the surface. This effectively increased the resolution of the data normal to the blade surface, but introduced error due to streamwise gradients in the boundary layer profile. Because the boundary layer was relatively thin, streamwise variations were ignored.

Figure 9 shows boundary layer profiles along the suction side blade chord at the 0.7 radius of Propeller 4119 at the effective advance coefficient of 0.806 for the low Reynolds number case (7.3×10^5). The vertical scale for each profile represents distance normal to the surface. The boundary layer developed in a fashion typical of a planar wing section, with laminar flow occurring up to around midchord. the point of transition is somewhat ill-defined because of insufficient chordwise resolution and possible chordwise fluctuation in the transition point which would be time-averaged over the duration of run. Typical turbulent boundary layer development occurs at the trailing edge region.

Measured boundary layer parameters were compared to calculations using a two-dimensional procedure of Cebeci (1978). A faired pressure distribution from the measured results in Figure 8 was supplied as input to the calculation procedure. Figure 10 shows comparisons of the measured and calculated values of displacment thickness, δ^*, and shape factor, H. The calculations were performed using prescribed transition locations of x_c equal to 0.5 and 0.6.

The correlation of displacement thickness shown in Figure 10a was reasonably good in the laminar flow region, with an underpredicted growth in boundary layer thickness in the turbulent region aft of midchord. Near the leading edge the measured displacement thickness of blade one was greater than calculated, possibly due to localized leading edge separation. Blade three was noticeably closer to the calculated values aft of midchord, which indicates blade-to-blade differences in geometry that will result in noticeable differences in boundary layer development.

The measured shape factor distribution over the chord resembles the calculated distribution in a general sense as shown in Figure 10b. Through the transition region the measured shape factors decreased less abruptly than predicted. Also there is significant

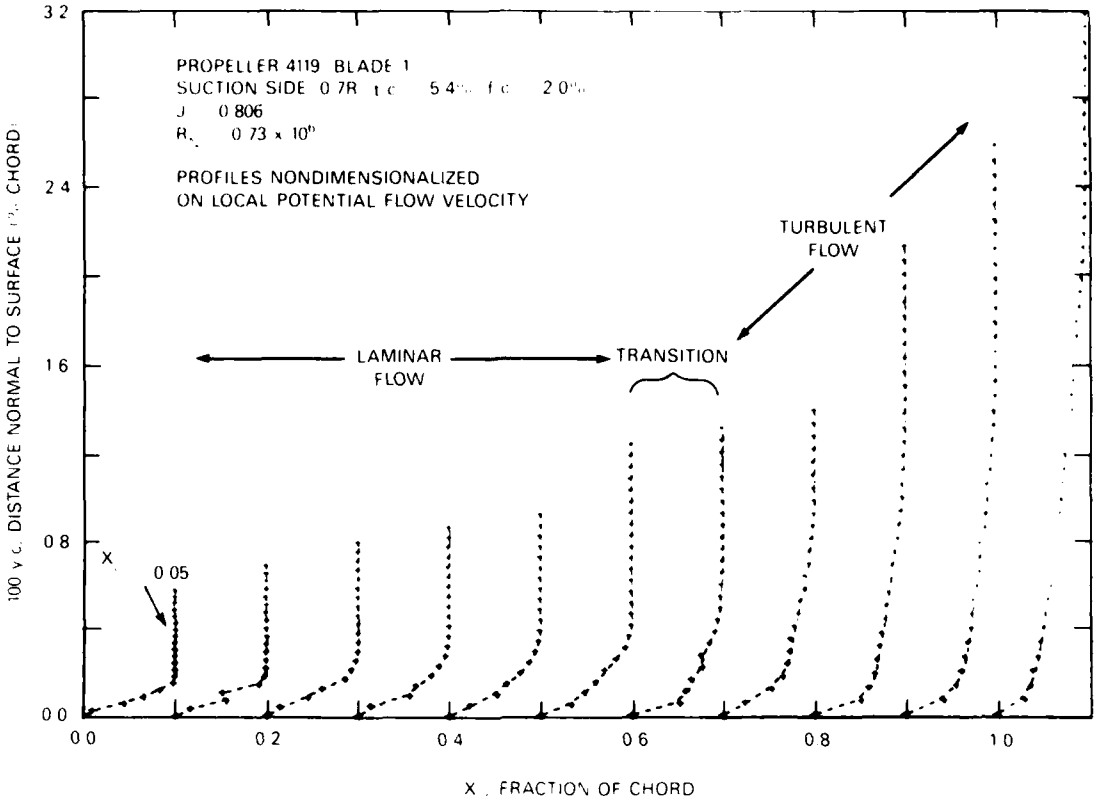

Figure 9. Measured Streamwise Boundary Layer Growth on Propeller 4119 0.7R Suction Side

scatter, blade to blade, in the transition region. The discrepancies observed between measured and calculated values of δ^* and H could be due to three dimensional boundary layer effects that are not accounted for in the two dimensional calculations. Unfortunately, the error associated with the location of the boundary surface prohibits detailed analysis of the blade boundary layer. Improved blade angle resolution will result in more precise measured boundary layer profiles.

3.5 Measurement of Turbulence Intensity

A measurement of the turbulence intensity in the streamwise component of the blade boundary layer was obtained from the standard deviation of the measured velocity samples recorded at each blade angular position. The turbulence intensity,

$$\sqrt{\overline{(V_\phi(i) - V_\phi)^2}}$$

was referenced to the moving blade and nondimensionalized by V_R, the resultant inflow to the blade section. A typical distribution of turbulence intensity across a turbulent boundary layer measured on Propeller 4119 is shown in Figure 11. The maximum turbulent intensity of about 10 percent is comparable to typical airfoil data. The turbulence intensity in the potential flow region away from the blade surface is approximately 1.5 percent relative to the moving blade.

When the turbulence intensity is nondimensionalized on advance speed, V_A, substantially larger turbulence levels occur. In this case values in Figure 11 would be uniformly increased by a factor of 2.8 resulting in maximum turbulence intensities of about 25 percent. The relatively high turbulence levels (relative to freestream speeds) that would be measured downstream of the propeller are produced by typical turbulent boundary layer growth on blade surfaces moving at speeds substantially higher than the freestream velocity. Therefore, with the absence of blade flow separation, propellers operating at higher advance coefficients would generally produce less downstream turbulence in the blade viscous wakes.

3.6 Flow Visualization of the Blade Surface Streamlines

After completion of the LDV measurements about Propeller 4119 blade surface flow visualization studies were conducted at the two Reynolds numbers tested. An oil dot technique was used in which a mixture of 90 weight gear oil and orange fluorescent pigment was applied with a drafting pen in a matrix of dots on the blade surface. The propeller was then run up to speed in the tunnel allowing the oil to spread from the dots at the desired test condition for approximately 30 seconds to a minute. When the propeller rotation and tunnel speed were ini-

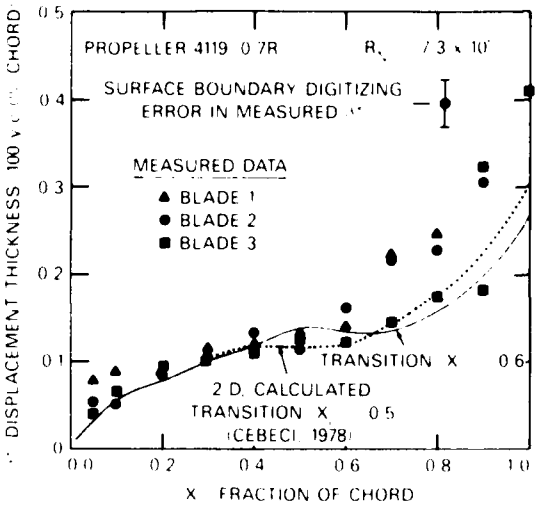

Figure 10a Displacement Thickness

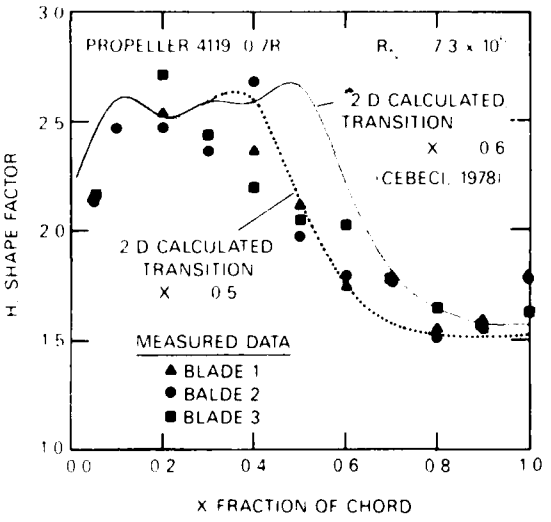

Figure 10b Shape Factor

Figure 10 Comparison of Measured Boundary Layer Parameters With 2 D Calculations

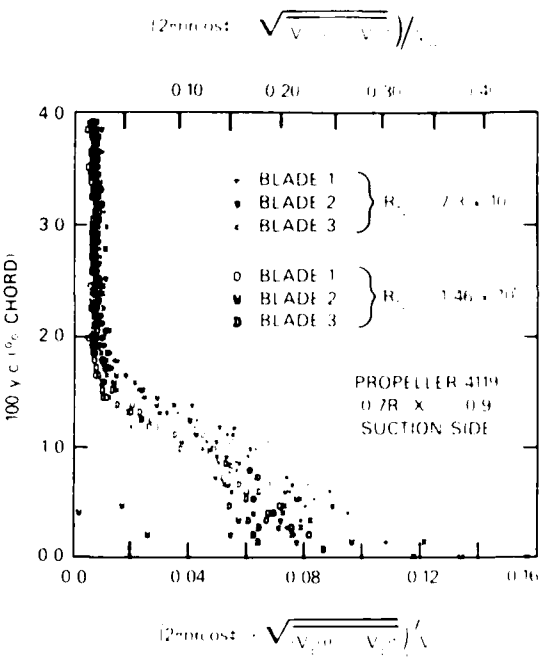

Figure 11 Streamwise Turbulence Intensity Through the Blade Boundary Layer

tially started, the tunnel speed generally lagged behind shaft rotation, so that the propeller operated at low advance speed in a transient fashion. Therefore, the initial 20 percent of the extended oil line was generally ignored. After the oil had extended completely from the dot, it was sufficiently fixed on the blade so that the running down of the shaft and water speed did not influence the oil pattern on the blade.

Figure 12 shows the results of the blade surface flow visualization conducted on Propeller 4119. Significant outward radial flow was observed over most of the blade, with a change in the surface streamline direction occurring towards the trailing edge.

Surface flow patterns of this sort have been investigated by Meyne (1972) and Kuiper (1978) and have been related to laminar and turbulent boundary layer development on a rotating disk. In laminar flow the surface streamline direction, β, on a rotating disk is 40 degrees from the circumferential direction, while in turbulent flow the angle is reduced to 11 degrees. The large difference in surface flow direction between laminar and turbulent boundary layer flow has been used qualitatively to determine regions on the propeller blades where laminar and turbulent flow occur. Large outward radial surface flow is associated with laminar boundary layer occurrence. When the surface flow direction changes to be oriented closer to the circumferential direction, the transition to a turbulent boundary layer is thought to occur.

The interpretation of surface flow direction should be considered relative to the local direction of the potential flow streamlines. In the midspan region of the blade the potential flow direction is approximately in the circumferential direction, so that qualitative boundary layer characteristics can be determined. Near the tip of the blade, strong radial flow velocities occur making qualitative interpretation difficult. If the potential flow streamlines were known, one could determine the angle β between the potential flow streamline and the surface streamlines from Figure 12.

Figures 12a and 12b show the surface streamline directions on the suction side of Propeller 4119 at the low Reynolds number

Figure 12a Suction Side. $R_c = 7.3 \times 10^5$

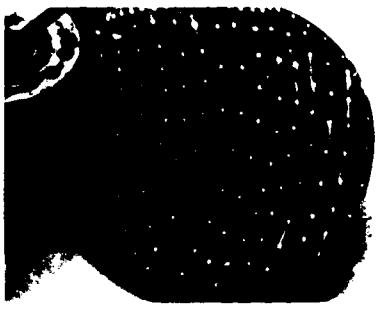

Figure 12d Suction Side. $R_c = 7.3 \times 10^5$ With Leading Edge Trip Wire

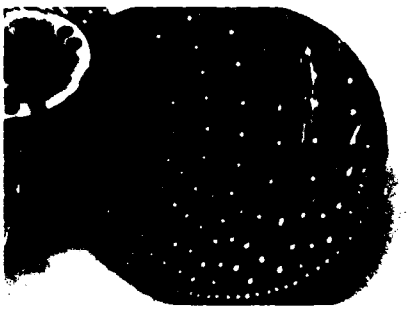

Figure 12b Suction Side. $R_c = 7.3 \times 10^5$

Figure 12e Suction Side. $R_c = 1.46 \times 10^6$

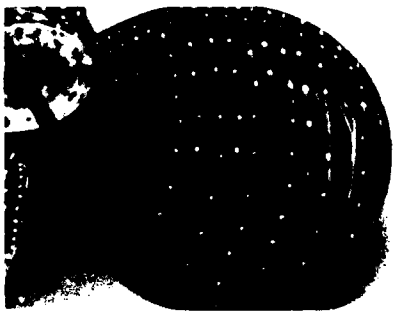

Figure 12c Pressure Side. $R_c = 7.3 \times 10^5$

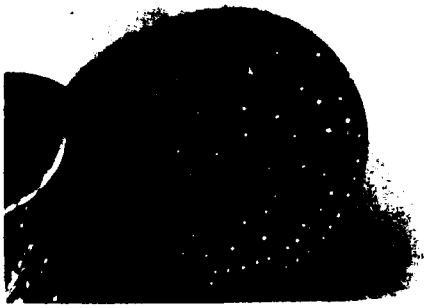

Figure 12f Pressure Side. $R_c = 1.46 \times 10^6$

Figure 12 Blade Surface Flow Visualization on Propeller 4119 Using Oil Dot Technique

tested, 7.3×10^5. Significant laminar flow appears with transition occurring around midchord at the 0.7 radius. This result correlates well with the measured boundary layer profiles shown in Figure 9. Figure 12e shows the surface flow on the suction side at the higher Reynolds number tested, 1.46×10^6. At 0.7 radius transition is estimated to occur around 30 percent chord. Transition has migrated forward as expected but significant laminar flow still occurs at the inner radii.

Figure 12c and 12f show the surface flow on the pressure side of the blade at the two Reynolds numbers tested. Again, significant laminar flow occurs over much of the blade at low Reynolds number, with transition shifting towards the leading edge at the higher Reynolds number run.

Figure 12d shows the blade surface flow on the suction side of the blade at the low Reynolds number condition with a 0.010 inch (.25mm) diameter trip wire attached near the leading edge from the 0.3 radius to the 0.7 radius. Downstream of the trip wire turbulent flow appeared to occur, but laminar flow persisted outboard of the trip wire from the 0.7 to 0.8 radii. No boundary layer measurements were made when trip wires were applied to the blades. In the future the LDV techniques described could be used to quantify the effects of boundary layer trips to simulate full scale Reynolds number flow similar to work done by McCarthy, et al. (1976) on axisymmetric bodies.

3.7 Qualitative Boundary Layer Measurements at Off Design Conditions

During the initial exploratory tests with the propeller boundary layer LDV system, qualitative measurements using a storage oscilloscope were conducted on propellers operating at off design conditions. An unskewed four bladed propeller, with wide, thin blades was used for these initial tests. Design J for this propeller was approximately 0.9 and qualitative measurements were obtained at J values of 0.38, 0.6 and 1.03.

Figure 13 Qualitative Velocity Measurements in the Pitch Line Direction on a Four Bladed Propeller at Off Design Conditions at 0.7 Radius

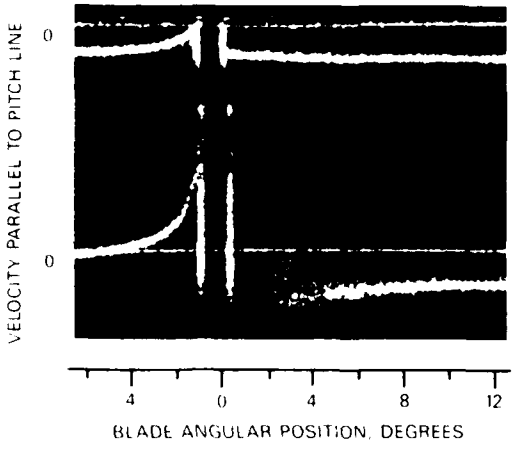

Figure 13a 2% Chord on Suction Side of Blade Top J = 1.03 Bottom J = 0.38 Boundary Layer Flow

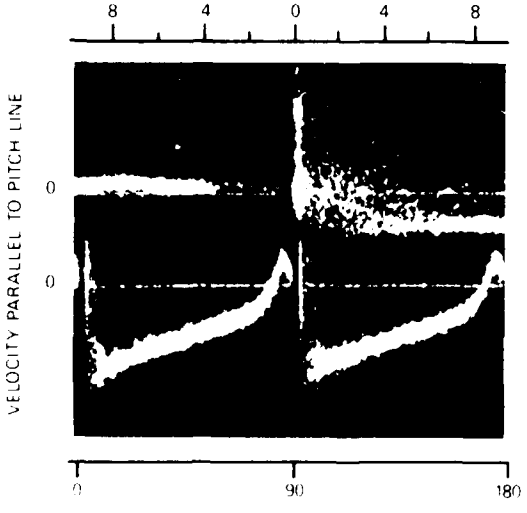

Figure 13b 10% Chord on Suction Side of Blade J = 0.38 Top Boundary Layer Flow Bottom Blade to Blade Potential Flow

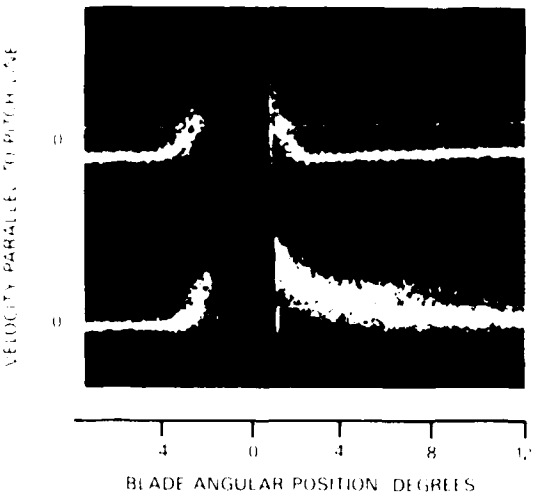

Figure 13c 87% Chord on Suction Side of Blade Boundary Layer Flow Top J = 1.03 Bottom J = 0.38

Velocity measurements near the leading edge of the blade at the low advance coefficients of 0.38 and 0.6 showed localized leading edge separation. During these tests, velocity was measured in the forward direction parallel to the pitch line of the propeller. Figure 13a shows the local blade velocity at a position corresponding to 2 percent chord on the suction side of the blade at the 0.7 radius. At the high J=1.03, low loading condition, the angle of attack of the section is small and the flow is attached on both sides of the blade. At the low J condition, the section is at a relatively high angle of attack inducing a large velocity difference between the suction and pressure sides of the blade. The potential flow velocity approaching the suction side of the blade appears to disintegrate producing large flucuations in velocity near the surface, associated with a region of separated flow. Figure 13b shows velocity profiles corresponding to the 10 percent chord position on the suction side. The top trace shows the local boundary layer flow indicating, again, large velocity fluctuations on the suction side of the blade. It is not obvious whether the boundary layer is attached or separated on the suction side at this chord position. The blade to blade potential flow in the lower trace shows the disintegration of the potential flow velocity near the suction side surface. Figure 13c shows the boundary layer flow at the 87 percent chord position at the high and low J conditions. At low J, in the lower trace, the suction side boundary layer appears turbulent and attached with a lower level of velocity fluctuations than observed close to the leading edge. The upper trace, corresponding to the J=1.03 condition, shows a much thinner turbulent boundary layer resulting from a more favorable chordwise pressure distribution and a smaller or no region of leading edge separation.

The effects of leading edge separation were discussed extensively by Greeley and Kerwin (1982) in relation to propellers. Generally, a long separation bubble extending over an appreciable fraction of the chord will reduce the suction peak predicted at the leading edge from potential flow theory. From Figure 13b, this appeared to be occurring. To check this, qualitative comparisons were made between measured and predicted velocity profiles through the 4 percent chord position of the four bladed propeller tested. Figure 14 shows the qualitative comparisons of measured results with PSF-2 (Greeley, 1982). The potential flow calculation shows significant peak velocities on both the suction and pressure sides of the blade. The measured result shows no suction side peak, implying a separation bubble occurring and reducing the magnitude of the potential flow velocity near the leading edge.

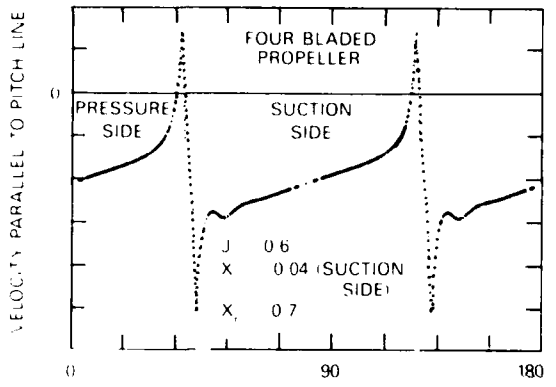

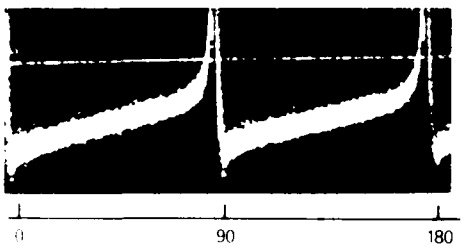

Figure 14 Qualitative Comparison of Measured Velocity Parallel to Pitch Line With Calculated Values Using PSF-2 and FPV-10 at 4% Chord

From the measured result, an approximate suction side surface velocity could be generated by straight line extrapolation of the potential flow velocity approaching the suction side of the blade.

3.8 Field Point Velocity Measurements With Sheared Onset Flow.

Velocity measurements were made ahead of a propeller operating in a sheard axisymmetric onset flow. This investigation was intended to compare measured performance with predictions using program PSF-2 of Greeley (1982) applied to a radially varying inflow.

The axisymmetric sheared wake was generated in the DTNSRDC 24-inch water tunnel using a 3 foot (0.9m) long, 6 inch (15.2 cm) diameter cylinder with an attached tail cone faired into the hub of the propeller. Also, an additional wake generator was used comprised of nine concetric rings 0.125 inches (3.2 mm) thick and 5 inches (12.7 cm) long mounted around the cylinder approximately 1.5 diameters ahead of the propeller. DTNSRDC Model Propeller 4645, a skewed, seven bladed, wake adapted propeller similar to that described by Wilson (1982) and Valentine and Chase (1976) was used for these tests.

Test conditions in the tunnel were set using thrust identity with an approximate design thrust coefficient, K_T = 0.28. Field point velocity measurements of axial and tangential velocity, V_x and V_t, were performed ahead of the operating propeller at an axial plane as close to the propeller as possible. Because of the aft rake of the blade sections, this resulted in measurements at the leading edge at the 0.3 radius and progressively further from the leading edge with increasing radius. A nominal inflow wake was determined by removing the propeller and measuring the axial inflow velocity, V_x, at the same measurement plane and at the same tunnel impeller rotation speed.

Programs PSF-2 and FPV-10 were used to predict the propeller's performance and field point velocities across the propeller disk.

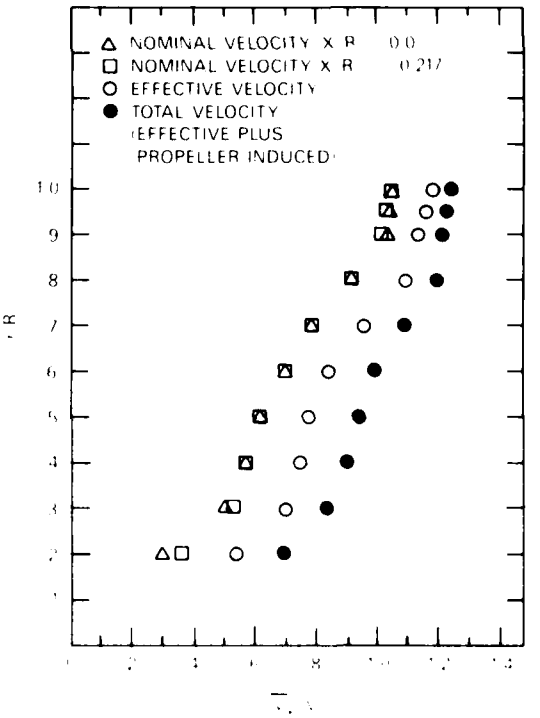

Figure [illegible] Comparison of Effective Wake From Propeller [illegible] Measured Circumferential Mean Velocity Across Propeller [illegible] Sheared Wake

The effective wake into the propeller was determined using PSF-2 and FPV-10 together with the experimental data obtained ahead of the propeller. Initially, the measured nominal wake was used as input to PSF-2 and FPV-10. The resultant calculated circumferential average propeller induced velocity at each radius was then subtracted from the measured total velocity leaving the estimated effective wake. This procedure was repeated for three iterations until the computed total velocity matched the measured values. Figure 15 shows the nominal, total and final effective wake distributions. It has been shown by Huang (1976) that the nominal and effective wake converge at a point beyond the propeller tip. The present results do not show this trend, possibly because of the confined flow in the water tunnel.

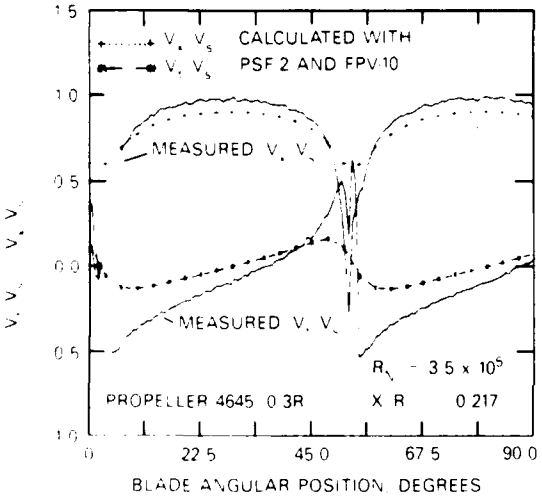

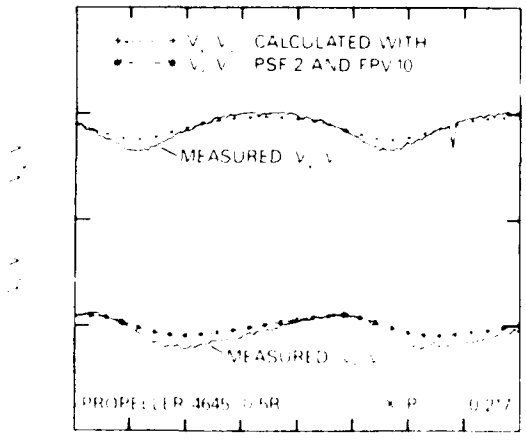

Predictions of the field point velocity distributions were compared with measured total velocity across the propeller disk. Figure 16a shows comparisons of V_x and V_t at 0.3 radius. The calculation underpredicts the circumferential variation of both velocity components. A possible explanation is the inaccuracies of thin wing theory in accounting for the influence of blade thickness close to the leading edge. At the 0.3 radius, the blade section was relatively thick and the measurements were obtained at the leading edge. Figure 16b shows comparisons at 0.5 radius. There, the blade section was thinner, and the measurement was sufficiently distant from the leading edge to avoid inaccuracies in the modeling of thickness effects, but the calculated result also underpredicted the measured peak to trough circumferential variation.

Comparison was also made of measured and predicted thrust. Initially, predictions were made of the measured open water performance of Propeller 4645 showing agreement to within 2 percent near its design condition. With the same empirical wake input parameters as in uniform flow, the effective wake in shear flow was input resulting in a 12 percent overprediction of the measured thrust set in the tunnel. This was inconsistant with the underprediction of the circumferential variation of the field point velocity ahead of the propeller. The field point velocity correlation suggested that the predicted loading should be higher, while the predicted thrust was already too high. There may have been experimental errors in the thrust measurement, and possible asymmetry in the sheared inflow wake, but it's unlikely these would explain the large discrepancy observed. Possible reasons for the discrepancies are hypothesized as follows:

1. Lack of consideration of the three dimensional nature of the induced velocity components associated with the effective wake in shear flow.

2. Improper modeling of the flow through the propeller in sheared wakes using program PSF-2, especially the downstream wake structure.

3. At inner radii, use of thin wing theory to model thickness effects in PSF-2.

4. CONCLUDING REMARKS

The primary contribution of this paper is the introduction of a local flow measuring technique with a great potential to investigate a variety of propeller problems. A high resolution one component back scatter LDV system has been developed to measure flows about operating propellers. A small LDV measuring volume, high resolution optical shaft encoding, and computer data acquisition and analysis have permitted detailed velocity measurements forward, aft, and within the blade boundary layers of operating propellers. The following conclusions can be made concerning the experimental results described in this paper:

1. Good correlation of measured and predicted (Greeley 1982) field point velocities have been further validated ahead of operating propellers in uniform flow. Correlation of field point velocities in the slip stream show discrepancies believed to be due to boundary layer displacement effects not modeled by the prediction method.

2. Blade surface pressure distributions can be derived from LDV measurement of potential flow velocity at the blade surface. Correlations with calculations (Kim, 1984) have shown reasonable agreement with noticeable Reynolds number effects on pressure distribution that are attributed to displacement thickness effects.

3. Streamwise boundary layer measurements on the suction side of Propeller 4119 have shown substantial laminar flow at model scale Reynolds numbers. Location of transition determined from measured boundary layer profiles correlated well with oil dot surface flow visualization techniques. Measured boundary layer growth at mid-span of the blade was approximated well with two-dimensional boundary layer theory using the measured pressure distribution.

4. Measured streamwise turbulence intensity through the turbulent boundary layer shows a typical magnitude relative to the moving blade reference frame.

5. Local blade flow measurements at off-design, low J conditions show leading edge separation with a resulting reduction in potential flow suction peaks.

6. Field point velocity and thrust measurements for a propeller operating in a sheared wake show an inconsistancy between measured and calculated results possible due to improper wake modeling in sheared flow and/or the three dimensionality of the effective wake.

REFERENCES

Cebeci, T. (1978): A Computer Program For Calculating Incompressible Laminar and Turbulent Boundary Layers on Plane and Axisymmetric Bodies with Surface Roughness. Report No. TR-78-1, California State University at Long Beach, Long Beach, California.

Denny, S. (1968): Cavitation and Open Water Performance Tests of a Series of Propellers Designed By Lifing-Surface Methods. David W. Taylor Naval Ship Research and Development Center, Report No. 2878.

Greeley, S. and Kerwin, J.E. (1982): Numerical Methods for Propeller Design and Analysis in Steady Flow. SNAME TRANSACTIONS, Vol. 90.

Huang, T.T. and Groves, N.C. (1980): Effective Wake: Theory and Experiement, 13th ONR Symposium on Naval Hydrodynamics, Tokyo, Japan.

Kerwin, J.E. and Lee, C.S. (1978): Prediction of Steady and Unsteady Marine Propeller Performance by Numerical Lifting Surface Theory. SNAME TRANSATIONS, Vol. 86.

Kerwin, J.E. (1979): Propeller Field Point Velocity Program FPV-10. MIT Dept. of Ocean Engineering, Cambridge, Mass.

Kerwin, J.E. (1982): Flow Field Computation for Non-Cavitation and Cavitating Propellers. 14th ONR Symposium on Naval Hydrodynamics, Ann Arbor, Michigan.

Kerwin, J.E. (1979): Propeller Field Point Velocity Program FPV-10. MIT Dept. of Ocean Engineering, Cambridge, Mass.

Kerwin, J.E. (1982): Flow Field Computation for Non-Cavitation and Cavitating Propellers. 14th ONR Symposium on Naval Hydrodynamics, Ann Arbor, Michigan.

Kim, K.H. and Kobayashi, S. (1984): Pressure Distribution on Propeller Blade Surface Using Numberical Lifing-Surface Thoery. SNAME Propellers '84 Symposium, Virginia Beach, Virginia.

Kobayashi, S. (1981): Experimental Methods for Prediction of the Effect of Viscosity on Propeller Performance. Report No. 81-7. MIT Dept. of Ocean Engineering, Cambridge, Mass.

Kuiper, G. 91978): Scale Effects on Propeller Cavitation Inception. 12th ONR Symposium on Naval Hydrodynamics, Washington, D.C.

McCarthy, J.H., et al. (1976): The Roles of Transition, Laminar Separation, and Turbulence Stimulation in the Analysis of Axisymmetric Body Drag. 11th ONR Symposium on Naval Hydrodynamics, London.

Meyne, K. (1972): Untersuchung der Propellergrenzschichstreomung und der Eingluss der Reiburg auf die Propellerkenngroessen (Investigation of Propeller Boundary-Layer Flow and Friction Effects on Propeller Characteristics). Jahrbuch der Schiffbautechnischen Gesellschaft, Band 66, Also DTNSRDC translation 352.

Min, K.S. (1978): Numerical and Experimental Methods for the Prediction of Field Point Velocities Around Propeller Blades. Report No. 78-12, MIT Dept. of Ocean Engineering, Cambridge, Mass.

Valentine, D.T. and Chase, A. (1976): Highly Skewed Propeller Design For A Naval Auxilary Oiler (AO177). David W. Taylor Naval Ship Research and Development Center, Report No. DTNSRDC [illegible]-41-12.

[illegible], M.S., et al. (1981): Causes and [illegible] for Propeller-Excited Airborne [illegible] on a Naval Auxiliary Oiler. SNAME [illegible].

INITIAL DISTRIBUTION

Copies	
1	ARMY CHIEF OF RES & DIV
1	ARMY ENGR R&D LAB
3	CHONR
	1 Code 438
	1 Lib
	1 Lee
4	ONR BOSTON
4	ONR CHICAGO
4	ONR LONDON, ENGLAND
1	NRL
2	USNA
	1 Lib
	1 Johnson
1	NAVPGSCOL Lib
1	NROTC & NAVADMINU, MIT
1	NADC
5	NOSC
	1 1311 Lib
	1 6005
	1 13111 Lib
	1 2501/Hoyt
	1 Nelson
1	NWC
43	NAVSEA
	3 SEA 05H
	5 SEA 05R
	1 SEA 55
	3 SEA 55D
	3 SEA 55N
	1 SEA 55W
	3 SEA 56D
	1 SEA 56X
	3 SEA 56X1
	1 SEA 56X2
	3 SEA 56X4
	1 SEA 56X5

Copies	
	NAVSEA (Continued)
	1 SEA 56XP
	1 PMS-378
	1 PMS-380
	1 PMS-381
	1 PMS-383
	1 PMS-389
	1 PMS-391
	1 PMS-392
	1 PMS-393
	1 PMS-397
	1 PMS-399
	1 PMS-400
	1 SEA Tech Rep Bath, England
	2 DET NORFOLK (Sec 6660)
2	MMA
	1 Lib
	1 Maritime Res Cen
1	FAC 032C
1	MILITARY SEALIFT COMMAND (M-4EX)
1	NAVSHIPYD/PTSMH
1	NAVSHIPYD/PHILA
1	NAVSHIPYD/NORVA
1	NAVSHIPYD/CHASN
1	NAVSHIPYD/LBEACH
1	NAVSHIPYD/MARE
1	NAVSHIPYD/PUGET
1	NAVSHIPYD/PEARL
12	DTIC
2	HQS COGARD
1	US COAST GUARD (G-ENE-4A)
1	LC/SCI & TECH DIV

Copies	
8	MARAD
	1 DIV SHIP DES
	1 COORD RES
	1 Shubert
	1 Falls
	1 Dashnaw
	1 Hammer
	1 Lasky
	1 Siebold
2	NASA STIF
	1 DIR RES
1	NSF ENGR DIV Lib
1	DOT Lib
1	U BRIDGEPORT/URAM
2	U CAL BERKELEY/DEPT NAME
	1 NAME Lib
	1 Webster
1	U CAL SAN DIEGO/Ellis
2	UC SCRIPPS
	1 Pollack
	1 Silverman
1	U MARYLAND/GLENN MARTIN INST
1	U MISSISSIPPI/DEPT OF M.E.
4	CIT
	1 AERO Lib
	1 Acosta
	1 Plesset
	1 Wu
2	CATHOLIC U
	1 Lib
	1 von Kerczak
1	COLORADO STATE U/Albertson
1	U CONNECTICUT/Scottron
1	CORNELL U/Sears
1	FLORIDA ATLANTIC U OE Lib

Copies	
3	HARVARD U
	1 McKay Lib
	1 Birkhoff
	1 Carrier
2	U HAWAII/Bretschneider
1	U ILLINOIS/Robertson
3	U IOWA
	1 IHR/Kennedy
	1 IHR/Landweber
	1 IHR/Stern
2	Johns Hopkins U
	1 Phillips
	1 Inst Coop Res
1	U KANSAS CIV ENGR Lib
1	KANSAS ST U ENGR EXP/Lib
1	LEHIGH U FRITZ ENGR LAB Lib
1	LONG ISLAND U
4	U MICHIGAN/DEPT NAME
	1 NAME Lib
	1 Parsons
	1 Vorus
	1 Brockett
5	MIT
	1 BARKER ENGR Lib
	2 OCEAN ENGR/Kerwin
	1 OCEAN ENGR/Leehey
	1 OCEAN ENGR/Newman
3	U MINNESOTA SAFHL
	1 Killen
	1 Song
	1 Wetzel
2	STATE U MARITIME COLL
	S U ARL Lib
	1 ENGR DEPT
	1 INST MATH SCI
1	NOTRE DAME ENGR Lib

Copies	
5	PENN STATE U ARL 1 Lib 1 Henderson 1 Gearhart 1 Parkin 1 Thompson
1	PRINCETON U/Mellor
1	RENSSELAER/DEPT MATH
1	ST JOHNS U
1	VIRGINIA TECH
3	SWRI 1 APPLIED MECH REVIEW 1 Abramson 1 Burnside
1	BOEING ADV AMR SYS DIV
3	BOLT BERANEK AND NEWMAN 1 Brown 1 Jackson 1 Greeley
1	BREWER ENGR LAB
1	CAMBRIDGE ACOUS/Junger
1	CALSPAN, INC/Ritter
1	STANDFORD U/Ashley
1	STANDFORD RES INST Lib
3	SIT DAVIDSON LAB 1 Lib 1 Breslin 1 Tsakonas
1	TEXAS U ARL Lib
1	UTAH STATE U/Jeppson
2	WEBB INST 1 Ward 1 Hadler

Copies	
1	WHOI OCEAN ENGR DEPT
1	WPI ALDEN HYDR LAB Lib
1	ASME/RES COMM INFO
1	ASNE
1	SNAME
1	AERO JET-GENERAL/Beckwith
1	ALLIS CHALMERS, YORK, PA
1	AVCO LYCOMING
1	BAKER MANUFACTURING
2	BATH IRON WORKS CORP 1 Hansen 1 FFG7 PROJECT OFFICE
1	BETHLEHEM STEEL SPARROWS
3	BIRD-JOHNSON CO 1 Case 1 Ridley 1 Norton
2	DOUGLAS AIRCRAFT 1 TECHNICAL Lib 1 Smith
2	EXXON RES DIV 1 Lib 1 Fitzgerald
1	FRIEDE & GOLDMAN/Michel
1	GEN DYN CONVAIR ASW-MARINE SCIENCES
3	GIBBS & COX 1 TECH Lib 1 Olson 1 CAPT Nelson
1	GRUMMAN AEROSPACE/Carl

Copies	
1	TRACOR/HYDRONAUTICS 1 Lib
1	INGALLS SHIPBUILDING
1	INST FOR DEFENSE ANAL
1	ITEK VIDYA
1	LIPS/Kress
1	LITTLETON R & ENGR CORP/Reed
1	LITTON INDUSTRIES
1	LOCKHEED/Waid
1	MARITECH, INC/Vassilopoulis
2	HYDRODYNAMICS RESEARCH ASSOCIATES, INC 1 Cox 1 Scharar
1	NATIONAL STEEL & SHIPBUILDING
1	NEWPORT NEWS SHIPBUILDING Lib
1	NIELSEN ENGR/Spangler
1	NKF Associates/Noonan
1	NAR SPACE/Ujihara
12	ORI, INC 1 Bullock 1 Amato 10 Kobayashi
1	PROPULSION DYNAMICS, INC
1	PROPULSION SYSTEMS, INC
1	SCIENCE APPLICATIONS, INC/ Salvensen
1	GEORGE G. SHARP
1	SPERRY SYS MGMT Lib/Shapiro

Copies	
1	SUN SHIPBLDG 1 Lib
1	ROBERT TAGGART
2	TETRA TECH PASADENA 1 Chapkis 1 Furuya
1	UNITED TECHNOLOGIES, HAMILTON STANDARD DIV/Cornell

CENTER DISTRIBUTION

Copies	Code	Name
1	0120	Nakonechny
1	12	Dietz
1	15	W.B. Morgan
1	1503	Monacella
1	1506	Hawkins
1	1509	Powell
1	152	Lin
1	1521	Day
1	1521	Karafiath
1	1521	Hurwitz
1	1522	Dobay
1	1522	Nagle
1	1522	Remmers
1	1522	Wilson
1	154	McCarthy
1	1542	Huang
1	1542	Fry
1	1542	Groves
1	1542	Shen
10	1543	Jeffers
1	1543	Platzer
1	1543	Santore
1	1543	Wisler
1	1544	Peterson
1	1544	Boswell
1	1544	Caster

Copies	Code	Name
1	1544	Reed
1	1544	Fuhs
20	1544	Jessup
1	1544	Lin
20	1544	Schott
1	156	Cieslowski
1	1561	Feldman
1	1561	O'Dea
1	1563	Milne
1	1564	Cox
1	172	Krenzke
1	1720.6	Rockwell
1	19	Sevik
1	19	Strasberg
1	1905	Blake
1	194	Archibald
1	1962	Noonan
1	1962	Kilcullen
10	5211.1	Reports Distribution
1	522.1	TIC (C)
1	522.2	TIC (A)

GPO 914-821

DTNSRDC ISSUES THREE TYPES OF REPORTS

1. DTNSRDC REPORTS, A FORMAL SERIES, CONTAIN INFORMATION OF PERMANENT TECHNICAL VALUE. THEY CARRY A CONSECUTIVE NUMERICAL IDENTIFICATION REGARDLESS OF THEIR CLASSIFICATION OR THE ORIGINATING DEPARTMENT.

2. DEPARTMENTAL REPORTS, A SEMIFORMAL SERIES, CONTAIN INFORMATION OF A PRELIMINARY, TEMPORARY, OR PROPRIETARY NATURE OR OF LIMITED INTEREST OR SIGNIFICANCE. THEY CARRY A DEPARTMENTAL ALPHANUMERICAL IDENTIFICATION.

3. TECHNICAL MEMORANDA, AN INFORMAL SERIES, CONTAIN TECHNICAL DOCUMENTATION OF LIMITED USE AND INTEREST. THEY ARE PRIMARILY WORKING PAPERS INTENDED FOR INTERNAL USE. THEY CARRY AN IDENTIFYING NUMBER WHICH INDICATES THEIR TYPE AND THE NUMERICAL CODE OF THE ORIGINATING DEPARTMENT. ANY DISTRIBUTION OUTSIDE DTNSRDC MUST BE APPROVED BY THE HEAD OF THE ORIGINATING DEPARTMENT ON A CASE-BY-CASE BASIS.

END

FILMED

6-85

DTIC